Post-transcriptional monoadenylation by TENT2 terminates human RNA polymerase III transcript 3' end processing and promotes 7SL RNA biogenesis

AUTHORS

Cody Ocheltree, Blake Skrable, Anastasia Pimentel, Timothy Nicholson-Shaw, Suzanne R. Lee# and Jens Lykke-Andersen*

Department of Molecular Biology, School of Biological Sciences, University of California San Diego, La Jolla, CA, 92093, USA

Current address: Biology Department, Western Washington University, Bellingham, WA 98225

* To whom correspondence should be addressed. Tel: +1 858-822-3659; Email: jlykkeandersen@ucsd.edu

ABSTRACT

Small non-coding RNAs (sncRNAs) are subject to a variety of 3' end trimming and tailing activities during biogenesis, which dictate whether they undergo maturation or are instead subjected to degradation. To investigate the dynamics of human sncRNA 3' end processing at a global level we performed genome-wide 3' end sequencing of nascently-transcribed and steady state sncRNAs. This revealed widespread post-transcriptional adenylation of nascent sncRNAs, which came in two distinct varieties. One is characterized by oligoadenylation, which is transient, promoted by TENT4A/4B polymerases, and observed primarily on unstable snoRNAs and scaRNAs that are not fully processed at their 3' ends. The other is characterized by monoadenylation, which is broadly catalyzed by TENT2 and stably accumulates at the 3'-end of many RNA Polymerase-III-transcribed (Pol-III) RNAs as well as a subset of small nuclear RNAs. This monoadenylation event terminates 3' end uridylation/deuridylation dynamics characteristic of nascent Pol-III RNAs and, in the case of 7SL RNAs, prevents their accumulation with nuclear La protein and promotes their biogenesis towards assembly into cytoplasmic signal recognition particles.

INTRODUCTION

The vast majority of eukaryotic RNAs undergo post-transcriptional processing critical for their biogenesis into functional mature RNAs. RNA 3'-ends in particular are subject to a wide variety of processing events including exonucleolytic trimming by 3'-to-5' exonucleases, addition of post-transcriptional nucleotides by polymerases, or 3' end nucleotide modifications such as 2',3' cyclic phosphorylation or 2'O-methylation. Some of the most abundant RNAs in eukaryotic cells are small non-coding RNAs (sncRNAs), which perform a wide variety of critical functions in gene expression. The majority of sncRNAs undergo processing at their 3' ends after their initial transcription, which can impact sncRNA cellular localization and function. Moreover, 3' end trimming and tailing towards sncRNA maturation have been observed to occur in competition with degradation from the 3' end in a process thought to distinguish functional from non-functional molecules (1–5).

SncRNAs can be divided into distinct classes in terms of how their 3' ends are initially formed. One consists of RNA polymerase II-transcribed sncRNAs, such as spliceosomal snRNAs, whose nascent 3' ends form via co-transcriptional cleavage by the integrator complex (6–9). This cleavage results in short encoded 3'-end extensions, which subsequently undergo various degrees of trimming (1, 3, 4). A second class consists of snoRNAs and scaRNAs that are encoded within introns of protein-coding or non-coding genes (10). The 3' ends of these sncRNAs are formed by the process of splicing, which is followed by intron debranching and trimming to generate the mature molecules (11). A third class consists of

RNA Polymerase-III (Pol-III or Pol3)-transcribed RNAs, which are terminated at oligo(T) DNA termination sequences (12–14). The resulting 3′-uridine termini generally undergo subsequent trimming or extension to generate the mature RNAs (15–18).

A large number of exonucleases and polymerases participate in the processing of sncRNA 3' ends. Some of these function in RNA maturation while others promote degradation. For example, 3'-to-5' exonucleases TOE1, PARN, and USB1 promote 3' end maturation of a large variety of sncRNAs (19), whereas DIS3 exonucleases, either as components of the exosome (DIS3 or DIS3L in human) (20, 21), or acting on its own in the cytoplasm (DIS3L2) (22), promote RNA degradation. 3' end tailing by polymerases has also been associated with either maturation or degradation dependent on the polymerase and RNA. For example, oligo-uridylation of RNAs by Terminal Uridylyltransferases (TUT) 4 and 7 promote degradation by DIS3L2 in the cytoplasm (23, 24), whereas oligoadenylation of RNAs by Terminal Nucleotidyltransferases TENT4A and TENT4B is associated with degradation by the exosome in the nucleus (25). However, adenylation has also been associated with RNA maturation and stability. For example, monoadenylation by the Terminal Nucleotidyltransferase TENT2 has been observed to stabilize a subset of microRNAs (26, 27) and oligoadenylation has been proposed to promote 3' end maturation activities of PARN (2, 28, 29) and TOE1 (1, 3, 4). However, the general principles that govern these 3' end trimming and tailing events and how they drive the competition between nascent sncRNA maturation and degradation remain poorly defined.

Many Pol-III RNAs undergo dynamic trimming and tailing of the initial 3' oligouridine termini produced during transcription termination. For U6 and U6atac snRNAs, these dynamics are terminated by a 2',3' cyclic phosphorylation event subsequent to U-tail extension, which is

important for their maturation and stability (17, 30). Another subset of Pol-III RNAs (as well as some snRNAs) have been observed to undergo monoadenylation to varying degrees (31) and this monoadenylation has been observed to oppose 3' uridylation in vitro and in injected Xenopus oocytes (32). One example is 7SL RNAs, which serve as the central scaffold of the Signal Recognition Particle (SRP) that functions in the co-translational translocation of polypeptides into the endoplasmic reticulum (ER) (33, 34). Biogenesis of 7SL RNAs involves assembly with several SRP proteins in the nucleus prior to nuclear export and association with a final SRP protein component, SRP54, in the cytoplasm (35–37). In mammalian cells, 7SL RNA is known to be processed at the 3′ end with the removal of terminal uridines and the addition of a monoadenosine tail (18, 31), but how this may impact 7SL RNA biogenesis and assembly into the SRP is unknown.

In this study, we investigated the genome-wide dynamics of 3′ end processing of human sncRNAs by sequencing 3′ ends of nascent and steady state sncRNAs, 100-500 nucleotides in length. This revealed widespread sncRNA post-transcriptional A-tailing, which was observed in two forms. One consisted of transient oligo(A)-tails, which were observed primarily on partially-processed snoRNAs and scaRNAs, and correlated with instability rather than 3' end maturation. Another consisted of mono(A)-tailing, which stably accumulated on a large number of Pol-III RNAs and a subset of snRNAs. We identified TENT2 as a non-canonical polymerase that broadly monoadenylates Pol-III RNAs and snRNAs and find that mono(A)-tailing by TENT2 terminates the 3′-uridylation and deuridylation dynamics typical of Pol-III RNA biogenesis. Moreover, we present evidence that monoadenylation promotes 7SL RNA biogenesis by inhibiting 7SL RNA interaction with nuclear La protein and promoting the assembly into cytoplasmic SRP particles.

MATERIAL AND METHODS

Reagents

Dulbecco's Modified Eagle Medium (11965118); Fetal Bovine Serum (10437-028); penicillin/streptomycin (15140122) were purchased from Gibco. TRIzol (15596018); Sybr Gold staining (S11494); Turbo DNA-free kit (AM1907); FastAP (EF0654); RNaseOUT (10777019); Click-it nascent RNA capture kit (C10365); ExoSAP-IT (78200.200.UL); Superscript III (18080085); rabbit polyclonal anti-TENT2 antibody (PA5-65876); donkey anti-rabbit antibody conjugated to HRP (A16035); SuperSignal West Femto substrate (34096); pcDNA5/FRT/TO (V652020); Flp-In 293 T-REx cells (R78007); Lipofectamine 2000 (11668019); Fast SYBR Green master mix (4385612); Dynabeads Protein G (10004D); BCA assay kit (23225) were purchased from Thermo Fisher. RNA clean & concentrator columns (R1014) was purchased from Zymo Research. RiboCOP rRNA depletion kit (144) was purchased from Lexogen. PNK (M0201L); PEG 8000 (B0216); T4 RNA ligase (B0216); Q5 DNA polymerase (M0492L); Gibson assembly master mix (E2611S) were purchased from New England Biolabs. DMSO (D2650-5X5ML); Iodoacetamide (I1149-5G); 4-thiouridine (T4509-100MG) were purchased from Sigma-Aldrich. AffinityScript Reverse Transcriptase (600559); Tapestation D1000 Screentape (5067-5582); D1000 Sample Buffer (5067-5602) were purchased from Agilent. AMPure XP beads (A63880) were purchased from Beckman Coulter. Rabbit polyclonal anti-b-tubulin antibody (2146); rabbit IgG antibody (2729); mouse IgG1 antibody (5415) were purchased from Cell Signaling Technology. QuickExtract (QE09050) was purchased from Biosearch Technologies Incorporated. siLentFect reagent (703362) was purchased from Bio-Rad. cOmplete protease inhibitor tablet (4693132001) was purchased from Roche. Anti-La antibody (sc-80656) was purchased from Santa Cruz Biotechnology. Anti-SRP54 antibody (MA5-34835) was purchased from Invitrogen.

Mammalian cell culture

All cells were maintained in Dulbecco's Modified Eagle Medium (DMEM, Gibco) supplemented with 10% Fetal Bovine Serum (FBS, Gibco) and 1% penicillin/streptomycin (Gibco) at 37°C, 5% CO_2. Mycoplasma testing was routinely performed.

Global 3' end sequencing of nascent small RNAs

HEK293 T-REx cells were incubated with either 0.5 mM 5-ethynyl uridine (EU; Thermo Fisher) or an equivalent volume of DMSO for 2 hours and harvested in TRIzol reagent (Thermo Fisher). Total RNA was isolated according to the manufacturer's recommendation. Small RNA from 180 µg of total RNA was isolated by separation in a 9% polyacrylamide/6M urea denaturing gel. After Sybr Gold staining (Thermo Fisher), small RNAs between 100 and 500 nucleotides in length were excised and eluted with gel elution buffer (0.3 M sodium acetate pH 5.3, 1 mM EDTA, 0.1% SDS) by end-over-end rotation overnight at 4°C. Eluted small RNAs were purified by RNA clean & concentrator columns (Zymo Research). Genomic DNA was removed using Turbo DNA-free kit (Thermo Fisher) and ribosomal (r)RNAs were depleted using RiboCOP rRNA depletion kit (Lexogen) per manufacturer's recommendations. RNA samples were treated with FastAP (Thermo Fisher) in 25 µl total volume and subsequently PNK (NEB) in 100 µl total volume in order to remove RNA 5'- and 3'-phosphates. RNA samples were again purified using RNA Clean & Concentrator columns (Zymo Research). AG15N or AG16N RNA adaptors (1 µM, Supplementary Table S4) were ligated to the RNA 3' ends by incubation at 25°C for 90 minutes in a 40 µl reaction containing 9% DMSO (Sigma), ligase buffer (50 mM

Tris-HCl pH 7.5, 10 mM $MgCl_2$, 1 mM DTT), 1 mM ATP (Thermo Fisher), 16 units RNaseOUT (Thermo Fisher), 20% PEG 8000 (NEB), and 80 units T4 RNA ligase (NEB). RNA from ligation reactions were purified using RNA Clean & Concentrator columns (Zymo Research). In order to isolate nascent RNAs labeled with EU, a portion of each sample was processed with Click-it nascent RNA capture kit (Thermo Fisher) as previously described (3), while the remaining portion did not undergo nascent enrichment in order to represent the steady state population. To determine the effectiveness of the nascent enrichment step, two truncated exogenous b-globin RNA probes approximately 250 nucleotides in length were spiked in to samples prior to nascent extraction – one probe was *in-vitro* transcribed with a 1:20 ratio of 5-ethynyl-UTP:UTP in order to mimic the estimated nucleotide ratio in cell culture, while a second probe was *in-vitro* transcribed only with UTP (Supplementary Table S4). Reverse transcription of nascently-made RNAs was performed on-bead in a total of 20 µl with 0.5 µM AR17 primer (Supplemental Table 3), 12.5 nM spike-in probe primer (Supplementary Table S4), AffinityScript buffer (1X, Agilent), 10 mM DTT, 4 mM dNTPs, 12 units RNaseOUT (Thermo Fisher), and AffinityScript Reverse Transcriptase (1X, Agilent) at 55°C for 45 minutes, followed by 15 minutes incubation at 70°C and 5 minutes of incubation at 85°C to release cDNA. Reverse transcription of RNA representing steady state accumulation was performed in tandem. Excess primer and RNA were removed from cDNA samples by incubating with 3.5 µl ExoSAP-IT (Thermo Fisher) at 37°C for 15 minutes, then treated with 3 µl of 1M NaOH at 70°C for 12 minutes and subsequently neutralized with 3 µl of 1M HCl. cDNA was extracted with phenol:chloroform:isoamyl alcohol and precipitated with 0.1 volume of 3 M sodium acetate pH 5.3 and 2.5 volumes of ethanol. A 3Tr3 adaptor (Supplementary Table S4) was ligated to cDNA 3′-ends at a final concentration of 3.2 µM in a 20 µl reaction with 5% DMSO (Sigma), in

ligase buffer (50 mM Tris-HCl pH 7.5, 10 mM $MgCl_2$, 1 mM DTT), 1 mM ATP (Thermo Fisher), and 45 units T4 RNA ligase (NEB) at 25°C for 16 hours.

cDNA to be sequenced was amplified in two stages of Polymerase Chain Reaction (PCR) using Q5 DNA polymerase (NEB). For the first PCR reaction, the cDNA library was amplified using 3′ adaptor primer (AR17) and a primer complementary to the 5′ adaptor (RC_3Tr3) (Supplementary Table S4) for 8 cycles. The PCR product was purified by AMPure XP beads (Beckman Coulter) per manufacturer's recommendation. The second PCR reaction was performed using Illumina Truseq D50X and D70X primers (Supplementary Table S4) for 18 cycles. The library quality was monitored by qPCR for select genes and Tapestation (Agilent) analyses. The relative ratios of EU-labeled to unlabeled spike-in probe cDNA were compared via qPCR in both nascently-extracted samples and samples representing the steady state (Supplementary Table S4). 100 bp paired-end sequencing was performed on an Illumina Novaseq S4.

Sequencing data analyses

Fastq files were first subjected to 3′ adaptor and PCR duplicate removal using custom python scripts (https://pypi.org/project/jla-demultiplexer/). Residual Illumina adaptor sequence was removed with Cutadapt (38). Reads were mapped to the human genome (version hg38) using STAR 2.7.11b (39). A three-pass alignment strategy against a small RNA genome was used as previously described (4), but with a modification in order to improve the local alignment step which provides post-transcriptional nucleotide modification information. After performing a three-pass end-to-end alignment, which includes a 5′-hard clip of 10 nucleotides to facilitate

alignment of reads with post-transcriptional nucleotide modifications, the aligned reads were grouped by gene and re-converted into individual fastq files for each gene detected using bedtools (40) and samtools (41). Individual-gene fastq files were then re-aligned with a three-pass local alignment to single-gene genomic sequences corresponding to the gene each file was previously aligned to in the end-to-end alignment. Gene-specific 3′ end information and graphs were subsequently generated using Tailer (42) (https://github.com/TimNicholsonShaw/tailer) using the global alignment mode.

Gene-specific RNA 3′ end sequencing

RNA was isolated using TRIzol (Thermo Fisher) per manufacturer's recommendation. RNA was subsequently treated with DNase I (Zymo Research), purified with RNA Clean & Concentrator columns (Zymo Research), and AG15N or AG16N RNA adaptors were ligated to RNA 3′ ends as described above. Following RNA purification with RNA Clean & Concentrator columns (Zymo Research), cDNA was synthesized with Superscript III (Thermo Fisher) using the AR17 primer (Supplementary Table S4). Gene-specific RNA 3′ end sequencing libraries were generated using gene-specific forward primers (Supplementary Table S4) and the AR17 reverse primer (Supplementary Table S4) with Q5 polymerase (NEB). Libraries were sequenced on an Illumina MiSeq platform and analyzed as previously described (3).

CRISPR/Cas9 knockout cell lines

The human *Terminal Nucleotidyltransferase 2* (*TENT2)* gene was targeted with guide RNAs against PAM sites located in 3′-exon 2 and 5′-intron 2 (Supplementary Figure S4B and Table

S4). The guide RNA-containing constructs and Cas9 vector were prepared and transfected as described previously (43) into HEK293 T-REx cells. Cells were selected for transfection construct expression by fluorescence-activated cell sorting for GFP-positive fluorescence. GFP-positive cells were plated as single-cell colonies and evaluated for genomic deletion of *TENT2* sequence using primers flanking exon 2 and intron 2 (Supplementary Table S4). PCR products were cloned into the PX459 plasmid (43), transformed into DH5a *E. coli* and prepared for sanger sequencing following plasmid purification (QIAprep, Qiagen). Six sequencing reactions were performed per knockout clone. Two unique alleles were detected from clones A and B from three and five successful sanger sequencing reactions, respectively (Supplementary Figure S4B and Table S5). The loss of the exon 2 splicing junction is predicted to result in a premature stop codon. A loss of TENT2 protein expression for TENT2 KO clones but not Control clones was validated by western blotting (Supplementary Figure S4C). A control clone was derived from cells which were GFP-positive, but did not present evidence for TENT2 genomic deletion or absence of TENT2 protein.

Western blotting

Western blots were performed by separating proteins in SDS-polyacrylamide gels followed by transfer to nitrocellulose membranes using standard procedures. Membranes were incubated overnight at 4°C with rabbit polyclonal anti-b-tubulin antibody (2146, Cell Signaling Technologies) and rabbit polyclonal anti-TENT2 antibody (PA5-65876, Thermo Fisher) diluted 1:1,000 in TBS with 0.1% Tween 20 (TBST) and 3% bovine serum albumin (BSA). Secondary donkey anti-rabbit antibodies conjugated to HRP (Thermo Fisher) were diluted 1:10,000 in TBST with 3% BSA and incubated for two hours at room temperature. Protein was visualized

with SuperSignal West Femto substrate (Thermo Fisher) using an Odyssey Fc imaging system (LI-COR).

Generation of plasmid constructs and stable cell lines

Gibson assembly (New England Biolabs) was used to insert a cDNA copy of the human *TENT2* gene with a N-terminal-3XFLAG-tag sequence into the pcDNA5/FRT/TO (Thermo Fisher) plasmid, creating pcDNA5-3XFLAG-TENT2WT. The 3XFLAG-tag sequence alone was additionally inserted into pcDNA5/FRT/TO. Site-directed mutagenesis (New England Biolabs) was used to create a silent mutation in the coding sequence of *TENT2*, conferring siRNA resistance and creating pcDNA5-3XFLAG-TENT2WT-R. Site-directed mutagenesis was again used to mutate two codons (ATGGTGA>CTGGTGC), resulting in Asp to Ala mutations at residues 213 and 215 critical for nucleotidyltrasferase catalytic activity of TENT proteins, creating pcDNA5-3XFLAG-TENT2DADA-R (44). pcDNA5-3XFLAG, pcDNA5-3XFLAG-TENT2WT-R and pcDNA5-3XFLAG-TENT2DADA-R constructs were subsequently integrated into the insertion site of Flp-In 293 T-REx cells (Thermo Fisher) per manufacturer's recommendations in order to generate stable cell lines expressing 3XFLAG, 3XFLAG-TENT2WT-R and 3XFLAG-TENT2DADA-R under control of a tetracycline-inducible promoter. Stable cell lines were treated with 50 ng/ml tetracycline 24 hours prior to harvest in order to induce expression of 3XFLAG, 3XFLAG-TENT2WT-R, and 3XFLAG-TENT2DADA-R proteins. Plasmid sequences are available upon request.

To generate vectors for expression of exogenous 7SL1 RNA, genomic DNA from HeLa cells was isolated with QuickExtract (Biosearch Technologies Inc.) and the 7SL1 gene was amplified

by PCR with Q5 polymerase (NEB), 3% DMSO, and primers positioned 154 base pairs upstream of the first transcribed nucleotide and 39 base pairs downstream of the annotated 3′-end (Supplementary Table S4). The amplicon was cloned into the pUC19 plasmid using standard molecular cloning techniques. The 7SL1 sequence was subsequently altered by Q5 (NEB) PCR amplification using primers (Supplementary Table S4) to achieve site-directed mutagenesis in order to create a distinguishable nucleotide barcode from endogenous 7SL1. Two barcoded exogenous 7SL1 sequences were synthesized (Supplementary Table S4).

RNA interference and plasmid transfection

Two sequential knockdowns were performed using 40 nM of small interfering RNAs (siRNAs) custom ordered from Horizon Discovery (Supplementary Table S4), 72 hours and 24 hours prior to harvest. Knockdowns were performed with siLentFect reagent (Bio-Rad, 703362) according to the manufacturer's specifications. The control siRNA targeted luciferase mRNA.

Transient transfection of plasmid containing exogenous 7SL and U1 sequences was performed 18 hours prior to harvest with Lipofectamine 2000 (Thermo Fisher) according to manufacturer's recommendations.

qPCR assays

AR17 (Supplementary Table S4)-primed cDNA was amplified using Fast SYBR Green master mix (Thermo Fisher) containing ROX with 1 µM primers targeting RNAs of interest (Supplementary Table S4) in a 10 µL reaction. Technical duplicates were performed for each

sample. Reactions underwent 40 cycles of 95°C denaturation and 60°C annealing with the QuantStudio Real-Time PCR system (Thermo Fisher) using the Fast protocol. Primer products were validated by quantification of primer efficiency, melt curve, and visualization by agarose gel electrophoresis. Cq values were determined with QuantStudio analysis software using default detection. Relative levels were quantified using the $\Delta\Delta C_t$ method (45).

RNA immunoprecipitation

Control or TENT2 KO 293 T-REx cells were transfected with plasmid containing exogenous 7SL and U1 sequences 18 hours prior to harvest. Cells were harvested by scraping into ice cold PBS and flash frozen in liquid nitrogen. Cells were resuspended in ice-cold isotonic lysis buffer (50 mM Tris-HCl pH 7.5, 150 mM NaCl, 5 mM EDTA, 0.5% Triton X-100, 80 U/mL RNaseOut (Thermo Fisher), protease inhibitor tablet/10 mL (Roche)) and incubated with rotation for 20 minutes at 4°C. Cellular debris was pelleted at 13,000 *g* for 15 minutes at 4°C. The supernatant was briefly pre-cleared using Protein G beads (Thermo Fisher, 10004D) for 10 minutes at 4°C with rotation. Beads for immunoprecipitation were washed with bead wash buffer (PBS pH 7.4, 0.1% Tween 20) and subsequently incubated with anti-La antibody (Santa Cruz Biotechnology, sc-80656), anti-SRP54 antibody (Invitrogen, MA5-34835), rabbit IgG (Cell Signaling Technology, 2729), or mouse IgG1 (Cell Signaling Technology, 5415) antibody for 1 hour at 4°C with rotation, then washed with bead wash buffer. Sample protein was quantified with a BCA assay (Thermo Fisher). 1 mg of protein per sample was diluted 5-fold with ice-cold detergent dilution buffer (isotonic lysis buffer without Triton X-100) and incubated with antibody-bead complexes for 1 hour at 4°C with rotation. Samples were washed 5 times with ice-cold immunoprecipitation wash buffer (PBS pH 7.4, 0.1% Tween 20,

150 mM NaCl) at 4°C. RNA from input and immunoprecipitation material was extracted with TRIzol (Thermo Fisher) according to the manufacturer's recommendation.

Gene-specific 3′-end sequencing libraries were prepared as described above. Libraries were sequenced on an Illumina MiSeq platform.

SLAM-seq

Control or TENT2 KO 293 T-REx cell media was treated with 4-thiouridine [s4U] at a final concentration of 100 μM as previously described and incubated for 3 hours, then refreshed with 100 μM s4U-containing media and incubated for an additional 3 hours (46). Cells were harvested by scraping into ice cold PBS and flash frozen in liquid nitrogen. RNA was extracted with TRIzol (Thermo Fisher) according to the manufacturer's recommendation.

Following RNA extraction, samples were treated with either iodoacetamide (IAA) or dimethylsulfoxide (DMSO) for 15 minutes at 50°C as previously described (46). Gene-specific 3′-end sequencing libraries were prepared as described above. Libraries were sequenced on an Illumina MiSeq platform. Gene-specific alignments were performed using in-house scripts which permitted T>C conversions. The number of conversions for each read was quantified and reads with two or more conversions were subsequently analyzed as nascently-labeled reads (Supplementary Figure S4G).

Website Referencing

https://pypi.org/project/jla-demultiplexer - for analysis of Tailer-produced taildata files.

RESULTS

Global analysis of sncRNA 3' end dynamics reveals transient and stable post-transcriptional A- and U-tails

To globally investigate the dynamics of human sncRNA 3′-end processing we performed 3′-end sequencing of steady-state and nascently-transcribed sncRNAs, 100 to 500 nucleotides in length, from human embryonic kidney (HEK) 293TRex cells (Figure 1A and Supplementary Figures S1A and S1B). A wide variety of small RNAs were represented in both steady-state and nascent libraries (Supplementary Figure S1C). Since RNAs that undergo 3′-end processing during biogenesis are expected to show differences in 3' end nucleotide composition in the nascent versus the steady state populations, we compared 3' ends of individual RNAs in nascent and steady state. We first examined the dynamics of post-transcriptional A- and U-tailing. We hypothesized that sncRNA post-transcriptional processing may be linked to their mechanism of initial 3' end formation and therefore grouped sncRNAs according to their transcriptional origin as snoRNAs (including box H/ACA snoRNAs, box C/D snoRNAs and scaRNAs), snRNAs (including spliceosomal snRNAs and U3 and U8 snoRNAs) and Pol-III RNAs.

Post-transcriptional A-tailing was prevalent among nascent sncRNAs, particularly among Pol-III RNAs some of which saw A-tailing of over 50% of the nascent population (Figure 1B). SnRNAs and Pol-III RNAs that saw A-tailing were typically mono(A)-tailed, whereas, consistent with previous observations (29, 31), snoRNAs experienced significantly longer oligo(A) tailing (Figure 1C). Post-transcriptional uridylation was also observed for a subset of sncRNAs but at a much lower frequency than A-tailing, and was significantly less frequent

among snoRNAs than among snRNAs and Pol-III RNAs (Figures 1B and 1C). Of note, post-transcriptional uridylation of Pol-III RNAs can be difficult to detect given their oligo-uridine termination sequences which cannot be distinguished from post-transcriptional uridines unless U-tails are very long (see further analyses below). Post-transcriptional cytosine and guanosine tails were detectable at some sncRNAs but were very rare and were not further investigated here (Supplementary Figures S1D-F).

To monitor the dynamics of sncRNA A- and U-tailing, we next compared A- and U-tails in steady state versus nascent conditions. This revealed different dynamics for sncRNAs from different transcriptional origins. For snoRNAs, post-transcriptional A- and U-tailing was overwhelmingly transient, as evidenced by a significant shortening of A- and U-tails in steady state compared to nascent conditions (Figure 1D and 1E). By contrast, post-transcriptional A- and U-tails were generally stable for Pol-III RNAs, while snRNAs displayed more of a mixture of transient and stable tails dependent on the RNA species (Supplementary Table S1).

Transient A-tailing of snoRNAs is associated with instability

Post-transcriptional A- and U-tailing has previously been associated with promotion of RNA 3' end trimming (1–3, 28, 29, 47) or RNA degradation (3, 47–49) but the principles that dictate one fate over another remain unclear. To first analyze whether A- or U-tailing correlates with 3' end trimming for each group of sncRNAs, we assessed sncRNA 3' end trimming by monitoring changes in 3’-ends of RNAs in the steady state population compared to the nascent. As expected, we observed significant 3' end shortening of a majority of snRNAs and snoRNAs, while a majority of Pol-III sncRNAs saw little 3’-end

trimming overall (Figure 2A and Supplementary Figure S2A). This trimming was not restricted to removal of post-transcriptional tails as it generally extended into the genome-encoded sncRNA body (Figure 2B and Supplementary Figure S2B). If 3' end trimming is promoted by A- or U-tailing it is predicted that RNAs that show 3’ trimming also show A- or U-tailing that is transient. To test this prediction, we classified RNAs with transient A- or U-tailing as those that displayed a significantly ($p<0.05$) higher fraction of A- or U-tailed molecules in the nascent population as compared to steady state. This analysis revealed no significant difference between the 3' end trimming of transiently A- or U-tailed sncRNAs and the sncRNA population as a whole (Figure 2C and Supplementary Figure S2C).

We next assessed whether a correlation exists between 3’-end tailing and sncRNA stability. RNAs that are unstable are expected to be enriched in the nascent population over steady state. We therefore used the ratio of RNA abundance in the steady state over nascent population as a proxy for RNA stability. Multiple sncRNAs that are unstable by this measure showed high levels of A- or U-tailing in the nascent population (Figure 2D). Evaluating whether correlations exist between transient tailing and stability for individual groups of sncRNAs, in the case of snoRNAs, those that underwent transient A-tailing showed significantly lower steady state to nascent RNA ratios than the remainder of the snoRNA population suggesting that the transiently A-tailed population is unstable (Figure 2E). Consistent with previous observations by others (29, 50, 51), the transient snoRNA A-tails were found on snoRNAs not fully processed at their 3’-ends (Figure 2F), suggesting that oligo(A)-tailing and degradation targets snoRNAs that experience stalling in 3' end processing. In contrast to a previous study suggesting that oligoadenylation is specific to H/ACA box snoRNAs (29), we observed transient oligoadenylation of snoRNAs of all types (Supplementary Table S2). Other classes of RNAs showed very few transiently A-tailed

species and no evidence of associated instability (Supplementary Figure S2D). While there were too few transiently U-tailed sncRNAs to be analyzed in a similar manner, the few sncRNAs that were uridylated at 2.5% or greater ratios in the nascent population were, as a group, significantly less stable than other sncRNAs (Supplementary Figure S2E).

A large number of Pol-III RNAs acquire stable mono(A)-tails

We next turned our attention to the short post-transcriptional tails observed on Pol-III RNAs and snRNAs. In contrast to snoRNAs, which typically see transient A-tails, over half of observed Pol-III RNAs, as well as a smaller subset of snRNAs, accumulate post-transcriptional A-tails at significantly higher levels at steady-state than in the nascent population suggesting that these tails are stable (Figure 1D and 3A). Pol-III RNAs as a group accumulated with A-tails at steady state at a higher level than other sncRNAs (Figure 3B) and these A-tails were generally mono(A)-tails (Figure 3C). While a majority of Pol-III RNAs can be observed with post-transcriptional A-tails at steady state, only three (7SL1, 7SL2 and 7SL3 RNAs) accumulate with A-tails on more than half of the population (Figure 3D and Supplementary Table S3). Performing the same analysis for U-tailing revealed a subset of snRNAs that accumulate U tails in the steady state, as well as a select few snRNAs that see U-tails that are transient (Supplementary Figure S3).

To confirm the mono(A)-tailing observed in our global 3′-end sequencing data, we monitored 3' ends of a subset of Pol-III RNAs and snRNAs by gene-specific 3' end sequencing, with U1 snRNA serving as a mostly unadenylated control. Plotting the composition of post-transcriptional tails for these RNAs support the conclusion that these

RNAs see 3' monoadenylation at the steady state, ranging from ≈15% of the population for U11 snRNA to ≈70% for 7SL1 and 7SL2 RNAs (Figure 3E). As expected, the U1 snRNA negative control showed little post-transcriptional 3'-end tailing at steady state. These observations, taken together, demonstrate that mono(A) tails stably accumulate to the steady state on a large number of Pol-III RNAs as well as a subset of snRNAs.

The non-canonical polymerase Terminal Nucleotidyltransferase 2 (TENT2) broadly promotes Pol-III and snRNA 3' end mono(A)-tailing

To better understand how 3'-end monoadenylation may impact sncRNA processing or function, we sought to identify the enzymatic activity responsible for this modification. The non-canonical polymerases TENT4A and TENT4B have been previously observed to adenylate a large number of sncRNAs (2, 29, 47, 48, 52). To assess whether TENT4A/4B are responsible for the observed oligo(A)- and/or mono(A)-tailing of sncRNAs, we analyzed a published TENT4A/4B knockdown 3'-end RNA-seq dataset (53). Plotting the changes in sncRNA 3'-adenylation in control versus TENT4A/4B co-depletion conditions revealed that snoRNA adenylation was significantly decreased during TENT4A/4B knockdown (Figure 4A and Supplementary Figure S4A). This is consistent with previous reports of snoRNA adenylation by TENT4B (2, 29). By contrast, snRNA and Pol-III RNA A-tailing was not significantly impacted. Taken together, these observations implicate TENT4A/4B in the transient oligo(A)-tailing of snoRNAs, while the short A-tails observed on Pol-III RNAs and a subset of snRNAs appear to be added by different polymerase(s).

Previous studies identified the mouse protein Germ Line Development 2 (mGLD2) as an enzyme that participates in monoadenylation of 7SL RNA (27). To test whether the human homolog of mGLD2, TENT2, promotes sncRNA 3′-monoadenylation, we knocked out the *TENT2* gene in HEK 293T-REx cells. Following confirmation of *TENT2* knockout (Supplementary Figures S4B and S4C), we performed direct 3' end sequencing of a subset of Pol-III RNAs and snRNAs and observed a significant reduction in 3′-adenylation for all RNAs tested (Figure 4B and Supplementary Figure S4D). Adenylation was almost completely abolished for 7SK, Y1, Y3 and U11 RNAs, whereas for 7SL1, 7SL2 and U2 RNAs approximately half of the original 3′-adenylated population remained after TENT2 knockout. The impact of TENT2 on Pol-III RNA and snRNA adenylation was confirmed by siRNA-mediated depletion of TENT2 (Figure 4C and Supplementary Figure S4E), and by add-back of exogenous wild-type TENT2 versus catalytically inactive TENT2 (Figure 4D). 3' end sequencing of nascent 7SL and U2 RNAs isolated from TENT2 knockout and control cells revealed a similar impact on 3′-adenylation as observed at steady state, showing that the adenylated population resistant to TENT2 KO does not reflect a highly stable population generated prior to TENT2 KO (Supplementary Figures S4F and S4G). Thus, snRNAs and Pol-III RNAs are mono-adenylated by TENT2, with a subset of the 7SL and U2 RNA population adenylated by an additional unknown enzyme, which is not TENT4A/4B (Supplementary Figure S4H).

Mono(A)-tailing by TENT2 terminates the dynamic trimming and tailing of Pol-III RNA oligo(U)-termini

Adenylation has previously been observed to inhibit uridylation of tested Pol-III RNAs *in vitro* and in injected *Xenopus* oocytes (32). We therefore examined the impact of TENT2 on cellular

Pol-III RNA uridylation/deuridylation dynamics. Previous studies of select Pol-III RNAs have observed dynamic uridylation and deuridylation during their biogenesis (15–18, 54). Indeed, globally comparing Pol-III RNA 3' end uridine termini in our 3' end sequencing data for nascent and steady-state populations revealed significant trimming or tailing of a majority of Pol-III RNAs. While U6 and U6atac snRNAs, as expected, undergo 3' uridine extension during biogenesis, a majority of Pol-III RNAs experience significant trimming of 3' uridines (Figure 5A). Moreover, for all Pol-III RNAs, a subset of their population could be observed to have undergone post-transcriptional U-tailing (Figure 5B), showing that dynamic uridine trimming and tailing is a common feature of Pol-III RNA biogenesis.

To ask whether monoadenylation by TENT2 impacts post-transcriptional Pol-III RNA uridylation, we used direct sequencing to monitor the effect of TENT2 knockout on the number of post-transcriptional uridines at select Pol-III RNA 3' ends. This analysis revealed a significant increase in the number of post-transcriptional uridines on the tested Pol-III RNA 3' ends upon TENT2 knockout (Figure 5C). Moreover, consistent with the idea that mono(A)-tailing inhibits post-transcriptional uridylation, post-transcriptional uridines were significantly more commonly preceded by uridines than by adenosines on these RNAs (Figure 5D).

To test whether mono(A)-tailing by TENT2 also inhibits the trimming of Pol-III RNA 3' uridines, we measured the mean number of 3’-uridines, whether genome-encoded or post-transcriptional in origin, of Pol-III RNAs at the steady state in the presence or absence of TENT2 KO. This revealed a general reduction in the number of 3' end uridines of the tested Pol-III RNAs upon TENT2 KO, with the most highly adenylated Pol-III RNAs, 7SL1 and 7SL2 RNAs, showing significant shortening (Figure 5E). Taken together, these observations show

that mono(A)-tailing by TENT2 terminates Pol-III RNA 3' end uridylation dynamics by inhibiting both 3′-uridine tailing and trimming (Figure 5F).

TENT2 inhibits 7SL RNA association with La protein

Given that 7SL1 and 7SL2 RNAs are the most highly adenylated sncRNAs with over 70% of the population accumulating with mono-A-tails, we next asked whether mono(A)-tailing by TENT2 impacts 7SL RNA biogenesis. We first asked if mono(A)-tailing by TENT2 affects 7SL RNA accumulation. Examining 7SL RNA levels in the presence or absence of TENT2 showed no effect of TENT2 depletion on 7SL RNA steady state accumulation (Supplementary Figure S5A). Given that 7SL RNAs are highly stable molecules we also monitored the impact of TENT2 on the accumulation of transiently expressed exogenous 7SL1 RNAs. The exogenous 7SL1 RNAs, for reasons that are unclear, are less adenylated and more uridylated at the 3' end than endogenous 7SL RNAs and more dependent on TENT2 for their 3' adenylation (Supplementary Figures S5B-E). We therefore wondered whether the exogenous 7SL1 RNAs would be more dependent on TENT2 for their accumulation. However, TENT2 depletion did not impact the accumulation of exogenous 7SL1 RNAs as monitored by RNA sequencing (Supplementary Figure S5F). These observations suggest that TENT2 does not significantly impact 7SL RNA stability.

Another possible impact of 7SL RNA monoadenylation could be on its association with RNA-binding proteins. The abundant nuclear RNA binding protein La is known to have high affinity for RNAs with 3′-oligouridines (55–57) and has been previously observed in budding yeast to associate with 7SL RNA (58). Performing immunoprecipitation against La and

assessing associated 7SL RNA levels in the presence or absence of TENT2 revealed significantly increased 7SL RNA association with La in the absence of TENT2 (Figure 6A). Sequencing the 3' ends of the La-associated 7SL RNAs revealed a significant enrichment in 3' uridylated and de-enrichment in adenylated species as compared with the overall 7SL RNA population (Figure 6B), consistent with a preference of La for unadenylated 7SL RNAs. Moreover, exogenous 7SL1 RNAs were enriched in association with La over the endogenous 7SL RNAs (Figure 6C), consistent with their significantly lower levels of adenylation and higher levels of uridylation (Figure 6D and Supplementary Figure S5E). These observations taken together demonstrate that mono(A)-tailing by TENT2 terminates uridylation dynamics at 7SL RNA 3' ends and inhibits the association of 7SL RNAs with La protein, consistent with the known preference of La for RNAs with oligo-uridine 3'-termini. Other tested sncRNAs were not observed to be significantly enriched with La upon TENT2 depletion (Supplementary Figure S5G), perhaps reflecting the smaller fractions of these RNA populations that receive mono(A)-tails by TENT2.

Excessively uridylated 7SL RNAs are impaired in the final step of SRP assembly

La-associated RNAs have been reported to be retained in the nucleus (15, 55, 59–61). Given that the last step of SRP assembly, the association of 7SL RNA with SRP54, occurs in the cytoplasm we considered the possibility that association of 7SL RNA with La negatively impacts its subsequent assembly with SRP54. Given the preference of La for RNAs with three or more 3' terminal uridines (55–57), we tested the prediction that 7SL RNAs with three or more 3' end uridines should be de-enriched in their association with SRP54. Indeed, immunoprecipitation against SRP54 followed by 7SL RNA 3' end sequencing revealed a

significant de-enrichment of this population of molecules in association with SRP54 for both 7SL1 and 7SL2 RNAs (Figure 7A). This could be observed both in the presence or absence of TENT2 KO. A similar de-enrichment in association with SRP54 was observed for the exogenous 7SL1 RNAs with three or more 3' uridines (Figure 7B), and, consistent with their significantly higher levels of uridylation, exogenous 7SL1 RNAs showed significantly lower levels of association with SRP54 than endogenous 7SL RNAs (Figure 7C). The overall level of endogenous 7SL RNA associated with SRP54 was not significantly impacted by TENT2 KO (Figures 7D) as may be expected given the low fraction (<2%) of endogenous 7SL RNAs that contain three or more 3' uridines at steady-state (Figure 7A and Supplementary Figure S6A). However, the more extensively uridylated exogenous 7SL1 RNAs were de-enriched in association with SRP54 upon TENT2 KO (Figure 7D) and SRP54-associated exogenous 7SL RNAs could be observed to be significantly de-enriched for uridylated species (Supplementary Figure S6B). Taken together, these observations suggest that the monoadenylation of 7SL RNAs by TENT2, by terminating 3' end uridylation dynamics, prevents the association of 7SL RNAs with La, which in turn allows 7SL RNAs to assemble with SRP54 in the cytoplasm to complete SRP biogenesis (Figure 7E).

DISCUSSION

In this study we globally characterized the dynamics of human sncRNA 3′-end processing and the relation between post-transcriptional tailing and sncRNA maturation and degradation. We observed post-transcriptional A-tailing of nascent sncRNAs to be wide-spread and consist of two major types. One is characterized by transient oligo(A)-tailing, which was observed predominantly on nascent snoRNAs and scaRNAs that were not fully processed at their 3' ends (Figure 1 and Supplementary Figure S2D). This oligo(A)-tailing is carried out by non-canonical polymerases TENT4A/4B and associated with instability rather than maturation (Figure 2), consistent with the known link between TENT4A/4B and the nuclear exosome (47, 48, 52, 62, 63). The second type of sncRNA A-tailing is characterized by mono(A)-tailing found on a large number of Pol-III RNAs and a smaller subset of snRNAs, and, in contrast to oligo(A)-tailing, stably accumulates to the steady state (Figure 3). TENT2 is broadly responsible for the addition of these mono(A)-tails, although other polymerases appear to contribute as well (Figure 4), and mono(A)-tailing terminates uridylation/deuridylation dynamics at Pol-III RNA 3′-ends (Figure 5). Mono(A)-tailing of 7SL RNAs inhibits their interaction with La protein (Figure 6) and extensively uridylated 7SL RNAs, which are favored for La binding, are inhibited from assembling with the cytoplasmic SRP component SRP54 (Figure 7), suggesting that mono(A)-tailing of 7SL RNAs promotes proper SRP biogenesis.

Our observation of transient oligo(A)-tailing of snoRNAs that are not fully 3' end processed is consistent with previous evidence for snoRNA adenylation by TENT4B occurring in competition with deadenylation by the deadenylase PARN during snoRNA maturation (2, 3, 27). We observed that the transient oligo(A)-tailing of snoRNAs correlates with instability

rather than maturation (Figure 2E), which, together with the observation that tailing occurs primarily on snoRNAs that are not fully 3' end processed (Figure 2F), suggests that adenylation by TENT4A/4B promotes degradation of snoRNAs whose maturation stalls during 3' end processing. We observed transient A-tailing and associated instability for H/ACA and C/D box snoRNAs and scaRNAs alike, suggesting that this mechanism of regulation is broadly applicable to these RNAs (Supplementary Table S2). These observations suggest that the competition between adenylation by TENT4A/4B and deadenylation by PARN (2, 29) at snoRNA 3'-ends dictates whether these RNAs are processed to maturation or subjected to degradation. A similar mechanism has been observed to regulate telomerase RNA levels, whereby deadenylation by PARN protects TERT from degradation initiated by TENT4B-mediated oligoadenylation (48). Similar oligoadenylation/deadenylation dynamics have additionally been observed for miRNAs (64, 65) and snRNAs (1, 3, 4), suggesting that this is a widespread mechanism to control sncRNA expression.

The second type of post-transcriptional A-tailing that we observed consists of mono(A)-tailing, which we find is stable and widespread. Pol-III RNAs naturally terminate with 3'-uridines, and we observed significant further uridylation or deuridylation during biogenesis for a majority of Pol-III RNAs. These dynamics are exemplified by the well-studied U6 snRNA, where processing terminates once a five-nucleotide uridine tail is modified with a 2',3' cyclic phosphate (30, 66). The adenylation of Pol-III RNAs was previously observed to inhibit uridylation *in vitro* and in injected *Xenopus* oocytes (32). Indeed, our findings suggest that mono(A)-tailing provides a second cellular mechanism to terminate 3' end uridylation/deuridylation dynamics of Pol-III RNAs. TENT2, which we show is broadly responsible for adding the stable mono(A)-tail, has previously been observed to inhibit oligo(U)-mediated degradation of miRNAs in mice (26, 27). While it is possible that mono(A)-

tailing likewise stabilizes Pol-III RNAs, we did not observe evidence for decreased levels of Pol-III RNAs in the absence of TENT2. However, for the majority of Pol-III RNAs, mono(A)-tailing occurs on less than half of the population and it is therefore possible that the mono(A)-tailed population is insufficiently large to observe stabilization of the overall RNA populations.

We observed 7SL RNAs as the most highly mono(A)-tailed RNAs with over 70% of the population accumulating with mono(A)-tails at steady state. TENT2 is partly responsible for this adenylation, but our findings suggest that additional polymerase(s) are involved as well. This second polymerase could be PAP-g which has been previously shown capable of adenylating 7SL RNAs *in vitro*, though RNA specificity for the modification was not observed (67). Our observations that TENT2 depletion leads to increased association of 7SL RNAs with La and that extensively uridylated 7SL RNAs are impaired in assembly with SRP54 suggest that mono(A)-tailing by TENT2 promotes 7SL RNA biogenesis. TENT2 has been reported to localize in the cytoplasm of vertebrates (68) although there has been reports of additional localization in the nucleus in mouse and *Xenopus* (69, 70). Our observations on the impact of TENT2 on 7SL RNA La binding suggests that TENT2 is active in the nucleus of human cells. Given evidence from others that La protein association results in nuclear retention (15, 55, 59–61), the simplest interpretation of our observations is that 7SL RNAs that experience post-transcriptional uridylation are retained in the nucleus by La, which prevents them from assembling into mature SRP particles in the cytoplasm. In this scenario, mono(A)-tailing would terminate uridylation dynamics at the 7SL RNA 3' ends and promote SRP assembly by preventing La association (Figure 7D). Thus uridylation/deuridylation dynamics terminated by a 2',3' cyclic phosphorylation, as in the case of U6 and U6atac snRNAs, or by monoadenylation as observed here, may play an important role in Pol-III RNA biogenesis

akin to the role of adenylation/deadenylation dynamics in the maturation of snoRNAs and other sncRNAs. An important question for future studies is what drives these uridylation/deuridylation dynamics and monoadenylation decisions, and whether these dynamics control the decision of whether Pol-III transcripts are destined for maturation or degradation.

DATA AVAILABILITY

Global and gene-specific 3' end RNA sequencing data have been deposited to the Gene Expression Omnibus (GEO) (71) under accession numbers GSE287260 and GSE287259, respectively.

AUTHOR CONTRIBUTIONS

C.O. and J.L-A. conceptualized the project. C.O. performed all experiments. C.O., B.S., T.N-S. and S.R.L. produced key reagents. C.O., B.S., A.P., T.N-S. and J.L-A. performed data analyses. C.O. and J.L-A. wrote the manuscript.

ACKNOWLEDGEMENTS

SncRNA global 3'-end sequencing was conducted at the UC San Diego IGM Genomics Center utilizing an Illumina NovaSeq 6000 that was purchased with funding from a National Institutes of Health SIG grant (#S10 OD026929). We thank Kristen Jepsen and the Sanford Human Embryonic Stem Cell Core for assistance with Illumina platform sequencing. We

thank Triton Shared Computer Cluster (TSCC) for facilitating computationally-intensive analyses and staff for guidance. We thank Tiantai Ma for his synthesis of exogenous U1 plasmids.

FUNDING

This work was supported by National Institutes of Health (NIH) grant R35 [GM118069] awarded to J. L.-A.

CONFLICT OF INTEREST

The authors declare no competing financial interests.

REFERENCES

1. Lardelli,R.M., Schaffer,A.E., Eggens,V.R.C., Zaki,M.S., Grainger,S., Sathe,S., Van Nostrand,E.L., Schlachetzki,Z., Rosti,B., Akizu,N., *et al.* (2017) Biallelic mutations in the 3′ exonuclease TOE1 cause pontocerebellar hypoplasia and uncover a role in snRNA processing. *Nat Genet*, **49**, 457–464.

2. Son,A., Park,J.-E. and Kim,V.N. (2018) PARN and TOE1 Constitute a 3′ End Maturation Module for Nuclear Non-coding RNAs. *Cell Reports*, **23**, 888–898.

3. Lardelli,R.M. and Lykke-Andersen,J. (2020) Competition between maturation and degradation drives human snRNA 3′ end quality control. *Genes Dev.*, **34**, 989–1001.

4. Ma,T., Xiong,E.S., Lardelli,R.M. and Lykke-Andersen,J. (2024) Sm complex assembly and 5′ cap trimethylation promote selective processing of snRNAs by the 3′ exonuclease TOE1. *Proceedings of the National Academy of Sciences*, **121**, e2315259121.

5. Fatica,A., Morlando,M. and Bozzoni,I. (2000) Yeast snoRNA accumulation relies on a cleavage-dependent/polyadenylation-independent 3′-processing apparatus. *The EMBO Journal*, **19**, 6218–6229.

6. Baillat,D., Hakimi,M.-A., Näär,A.M., Shilatifard,A., Cooch,N. and Shiekhattar,R. (2005) Integrator, a Multiprotein Mediator of Small Nuclear RNA Processing, Associates with the C-Terminal Repeat of RNA Polymerase II. *Cell*, **123**, 265–276.

7. Egloff,S., Szczepaniak,S.A., Dienstbier,M., Taylor,A., Knight,S. and Murphy,S. (2010) The Integrator Complex Recognizes a New Double Mark on the RNA Polymerase II Carboxyl-terminal Domain*. *Journal of Biological Chemistry*, **285**, 20564–20569.

8. O'Reilly,D., Kuznetsova,O.V., Laitem,C., Zaborowska,J., Dienstbier,M. and Murphy,S. (2014) Human snRNA genes use polyadenylation factors to promote efficient transcription termination. *Nucleic Acids Research*, **42**, 264–275.

9. Rubtsova,M.P., Vasilkova,D.P., Moshareva,M.A., Malyavko,A.N., Meerson,M.B., Zatsepin,T.S., Naraykina,Y.V., Beletsky,A.V., Ravin,N.V. and Dontsova,O.A. (2019) Integrator is a key component of human telomerase RNA biogenesis. *Sci Rep*, **9**, 1701.

10. Dieci,G., Preti,M. and Montanini,B. (2009) Eukaryotic snoRNAs: A paradigm for gene expression flexibility. *Genomics*, **94**, 83–88.

11. Filipowicz,W. and Pogačić,V. (2002) Biogenesis of small nucleolar ribonucleoproteins. *Current Opinion in Cell Biology*, **14**, 319–327.

12. Nielsen,S., Yuzenkova,Y. and Zenkin,N. (2013) Mechanism of Eukaryotic RNA Polymerase III Transcription Termination. *Science*, **340**, 1577–1580.

13. Braglia,P., Percudani,R. and Dieci,G. (2005) Sequence Context Effects on Oligo(dT) Termination Signal Recognition by *Saccharomyces cerevisiae* RNA Polymerase III*. *Journal of Biological Chemistry*, **280**, 19551–19562.

14. Gao,Z., Herrera-Carrillo,E. and Berkhout,B. (2018) Delineation of the Exact Transcription Termination Signal for Type 3 Polymerase III. *Molecular Therapy - Nucleic Acids*, **10**, 36–44.

15. Simons,F.H., Rutjes,S.A., van Venrooij,W.J. and Pruijn,G.J. (1996) The interactions with Ro60 and La differentially affect nuclear export of hY1 RNA. *RNA*, **2**, 264–273.

16. Ciganda,M. and Williams,N. (2011) Eukaryotic 5S rRNA biogenesis. *Wiley Interdiscip Rev RNA*, **2**, 523–533.

17. Yamashita,S. and Tomita,K. (2023) Mechanism of U6 snRNA oligouridylation by human TUT1. *Nat Commun*, **14**, 4686.

18. Chen,Y., Sinha,K., Perumal,K., Gu,J. and Reddy,R. (1998) Accurate 3′ end processing and adenylation of human signal recognition particle RNA and alu RNA in vitro. *J Biol Chem*, **273**, 35023–35031.

19. Huynh,T.N. and Parker,R. (2023) The PARN, TOE1, and USB1 RNA deadenylases and their roles in non-coding RNA regulation. *Journal of Biological Chemistry*, **299**.

20. Lykke-Andersen,S., Tomecki,R., Jensen,T.H. and Dziembowski,A. (2011) The eukaryotic RNA exosome: Same scaffold but variable catalytic subunits. *RNA Biology*, **8**, 61–66.

21. Tomecki,R., Kristiansen,M.S., Lykke-Andersen,S., Chlebowski,A., Larsen,K.M., Szczesny,R.J., Drazkowska,K., Pastula,A., Andersen,J.S., Stepien,P.P., *et al.* (2010) The human core exosome interacts with differentially localized processive RNases: hDIS3 and hDIS3L. *EMBO J*, **29**, 2342–2357.

22. Belair,C., Sim,S. and Wolin,S.L. (2018) Noncoding RNA Surveillance: The Ends Justify the Means. *Chem. Rev.*, **118**, 4422–4447.

23. Ustianenko,D., Pasulka,J., Feketova,Z., Bednarik,L., Zigackova,D., Fortova,A., Zavolan,M. and Vanacova,S. (2016) TUT-DIS3L2 is a mammalian surveillance

pathway for aberrant structured non-coding RNAs. *The EMBO Journal*, **35**, 2179–2191.

24. Pirouz,M., Du,P., Munafò,M. and Gregory,R.I. (2016) Dis3l2-Mediated Decay Is a Quality Control Pathway for Noncoding RNAs. *Cell Rep*, **16**, 1861–1873.

25. Warkocki,Z., Liudkovska,V., Gewartowska,O., Mroczek,S. and Dziembowski,A. (2018) Terminal nucleotidyl transferases (TENTs) in mammalian RNA metabolism. *Philosophical Transactions of the Royal Society B: Biological Sciences*, **373**, 20180162.

26. D'Ambrogio,A., Gu,W., Udagawa,T., Mello,C.C. and Richter,J.D. (2012) Specific miRNA Stabilization by Gld2-Catalyzed Monoadenylation. *Cell Reports*, **2**, 1537–1545.

27. Katoh,T., Sakaguchi,Y., Miyauchi,K., Suzuki,T., Kashiwabara,S.-I., Baba,T. and Suzuki,T. (2009) Selective stabilization of mammalian microRNAs by 3' adenylation mediated by the cytoplasmic poly(A) polymerase GLD-2. *Genes Dev*, **23**, 433–438.

28. Moon,D.H., Segal,M., Boyraz,B., Guinan,E., Hofmann,I., Cahan,P., Tai,A.K. and Agarwal,S. (2015) Poly(A)-specific ribonuclease (PARN) mediates 3'-end maturation of the telomerase RNA component. *Nat Genet*, **47**, 1482–1488.

29. Berndt,H., Harnisch,C., Rammelt,C., Stöhr,N., Zirkel,A., Dohm,J.C., Himmelbauer,H., Tavanez,J.-P., Hüttelmaier,S. and Wahle,E. (2012) Maturation of mammalian H/ACA box snoRNAs: PAPD5-dependent adenylation and PARN-dependent trimming. *RNA*, **18**, 958–972.

30. Didychuk,A.L., Montemayor,E.J., Carrocci,T.J., DeLaitsch,A.T., Lucarelli,S.E., Westler,W.M., Brow,D.A., Hoskins,A.A. and Butcher,S.E. (2017) Usb1 controls U6 snRNP assembly through evolutionarily divergent cyclic phosphodiesterase activities. *Nat Commun*, **8**, 497.

31. Sinha,K.M., Gu,J., Chen,Y. and Reddy,R. (1998) Adenylation of small RNAs in human cells. Development of a cell-free system for accurate adenylation on the 3'-end of human signal recognition particle RNA. *J Biol Chem*, **273**, 6853–6859.

32. Chen,Y., Sinha,K., Perumal,K. and Reddy,R. (2000) Effect of 3' terminal adenylic acid residue on the uridylation of human small RNAs in vitro and in frog oocytes. *RNA*, **6**, 1277–1288.

33. Kellogg,M.K., Miller,S.C., Tikhonova,E.B. and Karamyshev,A.L. (2021) SRPassing Co-translational Targeting: The Role of the Signal Recognition Particle in Protein

Targeting and mRNA Protection. *International Journal of Molecular Sciences*, **22**, 6284.

34. Akopian,D., Shen,K., Zhang,X. and Shan,S. (2013) Signal Recognition Particle: An Essential Protein-Targeting Machine. *Annual Review of Biochemistry*, **82**, 693–721.

35. Jacobson,M.R. and Pederson,T. (1998) Localization of signal recognition particle RNA in the nucleolus of mammalian cells. *Proc Natl Acad Sci U S A*, **95**, 7981–7986.

36. Ciufo,L.F. and Brown,J.D. (2000) Nuclear export of yeast signal recognition particle lacking Srp54p by the Xpo1p/Crm1p NES-dependent pathway. *Current Biology*, **10**, 1256–1264.

37. Grosshans,H., Deinert,K., Hurt,E. and Simos,G. (2001) Biogenesis of the signal recognition particle (SRP) involves import of SRP proteins into the nucleolus, assembly with the SRP-RNA, and Xpo1p-mediated export. *J Cell Biol*, **153**, 745–762.

38. Martin,M. (2011) Cutadapt removes adapter sequences from high-throughput sequencing reads. *EMBnet.journal*, **17**, 10–12.

39. Dobin,A., Davis,C.A., Schlesinger,F., Drenkow,J., Zaleski,C., Jha,S., Batut,P., Chaisson,M. and Gingeras,T.R. (2013) STAR: ultrafast universal RNA-seq aligner. *Bioinformatics*, **29**, 15–21.

40. Quinlan,A.R. and Hall,I.M. (2010) BEDTools: a flexible suite of utilities for comparing genomic features. *Bioinformatics*, **26**, 841–842.

41. Li,H., Handsaker,B., Wysoker,A., Fennell,T., Ruan,J., Homer,N., Marth,G., Abecasis,G., Durbin,R., and 1000 Genome Project Data Processing Subgroup (2009) The Sequence Alignment/Map format and SAMtools. *Bioinformatics*, **25**, 2078–2079.

42. Nicholson-Shaw,T. and Lykke-Andersen,J. Tailer: A Pipeline for Sequencing-Based Analysis of Non- Polyadenylated RNA 3' End Processing.

43. Ran,F.A., Hsu,P.D., Wright,J., Agarwala,V., Scott,D.A. and Zhang,F. (2013) Genome engineering using the CRISPR-Cas9 system. *Nat Protoc*, **8**, 2281–2308.

44. Rissland,O.S., Mikulasova,A. and Norbury,C.J. (2007) Efficient RNA Polyuridylation by Noncanonical Poly(A) Polymerases. *Molecular and Cellular Biology*, **27**, 3612–3624.

45. Livak,K.J. and Schmittgen,T.D. (2001) Analysis of Relative Gene Expression Data Using Real-Time Quantitative PCR and the 2−ΔΔCT Method. *Methods*, **25**, 402–408.

46. Herzog,V.A., Reichholf,B., Neumann,T., Rescheneder,P., Bhat,P., Burkard,T.R., Wlotzka,W., von Haeseler,A., Zuber,J. and Ameres,S.L. (2017) Thiol-linked alkylation of RNA to assess expression dynamics. *Nat Methods*, **14**, 1198–1204.

47. Shukla,S. and Parker,R. (2017) PARN Modulates Y RNA Stability and Its 3′-End Formation. *Molecular and Cellular Biology*, **37**, e00264-17.

48. Tseng,C.-K., Wang,H.-F., Burns,A.M., Schroeder,M.R., Gaspari,M. and Baumann,P. (2015) Human Telomerase RNA Processing and Quality Control. *Cell Rep*, **13**, 2232–2243.

49. Sudo,H., Nozaki,A., Uno,H., Ishida,Y. and Nagahama,M. (2016) Interaction properties of human TRAMP-like proteins and their role in pre-rRNA 5′ETS turnover. *FEBS Letters*, **590**, 2963–2972.

50. Allmang,C., Kufel,J., Chanfreau,G., Mitchell,P., Petfalski,E. and Tollervey,D. (1999) Functions of the exosome in rRNA, snoRNA and snRNA synthesis. *The EMBO Journal*, **18**, 5399–5410.

51. van Hoof,A., Lennertz,P. and Parker,R. (2000) Yeast exosome mutants accumulate 3′-extended polyadenylated forms of U4 small nuclear RNA and small nucleolar RNAs. *Mol Cell Biol*, **20**, 441–452.

52. Wlotzka,W., Kudla,G., Granneman,S. and Tollervey,D. (2011) The nuclear RNA polymerase II surveillance system targets polymerase III transcripts. *EMBO J*, **30**, 1790–1803.

53. Lim,J., Kim,D., Lee,Y.-S., Ha,M., Lee,M., Yeo,J., Chang,H., Song,J., Ahn,K. and Kim,V.N. (2018) Mixed tailing by TENT4A and TENT4B shields mRNA from rapid deadenylation. *Science*, **361**, 701–704.

54. Mroczek,S. and Dziembowski,A. (2013) U6 RNA biogenesis and disease association. *WIREs RNA*, **4**, 581–592.

55. Stefano,J.E. (1984) Purified lupus antigen la recognizes an oligouridylate stretch common to the 3′ termini of RNA polymerase III transcripts. *Cell*, **36**, 145–154.

56. Teplova,M., Yuan,Y.-R., Phan,A.T., Malinina,L., Ilin,S., Teplov,A. and Patel,D.J. (2006) Structural Basis for Recognition and Sequestration of UUUOH 3′ Temini of Nascent RNA Polymerase III Transcripts by La, a Rheumatic Disease Autoantigen. *Molecular Cell*, **21**, 75–85.

57. Rinke,J. and Steitz,J.A. (1982) Precursor molecules of both human 5S ribosomal RNA and transfer RNAs are bound by a cellular protein reactive with anti-La Lupus antibodies. *Cell*, **29**, 149–159.

58. Leung,E., Schneider,C., Yan,F., Mohi-El-Din,H., Kudla,G., Tuck,A., Wlotzka,W., Doronina,V.A., Bartley,R., Watkins,N.J., *et al.* (2014) Integrity of SRP RNA is ensured by La and the nuclear RNA quality control machinery. *Nucleic Acids Research*, **42**, 10698–10710.

59. Jacks,A., Babon,J., Kelly,G., Manolaridis,I., Cary,P.D., Curry,S. and Conte,M.R. (2003) Structure of the C-Terminal Domain of Human La Protein Reveals a Novel RNA Recognition Motif Coupled to a Helical Nuclear Retention Element. *Structure*, **11**, 833–843.

60. Boelens,W.C., Palacios,I. and Mattaj,I.W. (1995) Nuclear retention of RNA as a mechanism for localization. *RNA*, **1**, 273–283.

61. Grimm,C., Lund,E. and Dahlberg,J.E. (1997) In vivo selection of RNAs that localize in the nucleus. *The EMBO Journal*, **16**, 793–806.

62. Rammelt,C., Bilen,B., Zavolan,M. and Keller,W. (2011) PAPD5, a noncanonical poly(A) polymerase with an unusual RNA-binding motif. *RNA*, **17**, 1737–1746.

63. Carneiro,T., Carvalho,C., Braga,J., Rino,J., Milligan,L., Tollervey,D. and Carmo-Fonseca,M. (2007) Depletion of the Yeast Nuclear Exosome Subunit Rrp6 Results in Accumulation of Polyadenylated RNAs in a Discrete Domain within the Nucleolus. *Molecular and Cellular Biology*, **27**, 4157–4165.

64. Jeong,H.-C., Shukla,S., Fok,W.C., Huynh,T.N., Batista,L.F.Z. and Parker,R. (2023) USB1 is a miRNA deadenylase that regulates hematopoietic development. *Science*, **379**, 901–907.

65. Shukla,S., Bjerke,G.A., Muhlrad,D., Yi,R. and Parker,R. (2019) The RNase PARN Controls the Levels of Specific miRNAs that Contribute to p53 Regulation. *Mol Cell*, **73**, 1204-1216.e4.

66. Lund,E. and Dahlberg,J.E. (1992) Cyclic 2′,3′-Phosphates and Nontemplated Nucleotides at the 3′ End of Spliceosomal U6 Small Nuclear RNA's. *Science*, **255**, 327–330.

67. Perumal,K., Sinha,K., Henning,D. and Reddy,R. (2001) Purification, characterization, and cloning of the cDNA of human signal recognition particle RNA 3′-adenylating enzyme. *J Biol Chem*, **276**, 21791–21796.

68. Barnard,D.C., Ryan,K., Manley,J.L. and Richter,J.D. (2004) Symplekin and xGLD-2 Are Required for CPEB-Mediated Cytoplasmic Polyadenylation. *Cell*, **119**, 641–651.

69. Nakanishi,T., Kubota,H., Ishibashi,N., Kumagai,S., Watanabe,H., Yamashita,M., Kashiwabara,S., Miyado,K. and Baba,T. (2006) Possible role of mouse poly(A) polymerase mGLD-2 during oocyte maturation. *Developmental Biology*, **289**, 115–126.

70. Rouhana,L., Wang,L., Buter,N., Kwak,J.E., Schiltz,C.A., Gonzalez,T., Kelley,A.E., Landry,C.F. and Wickens,M. (2005) Vertebrate GLD2 poly(A) polymerases in the germline and the brain. *RNA*, **11**, 1117–1130.

71. Barrett,T., Wilhite,S.E., Ledoux,P., Evangelista,C., Kim,I.F., Tomashevsky,M., Marshall,K.A., Phillippy,K.H., Sherman,P.M., Holko,M., *et al.* (2013) NCBI GEO: archive for functional genomics data sets—update. *Nucleic Acids Research*, **41**, D991–D995.

TABLES AND FIGURES

Figure 1 – Post-transcriptional A- and U-tails are transient on a subset of sncRNAs but stable on others

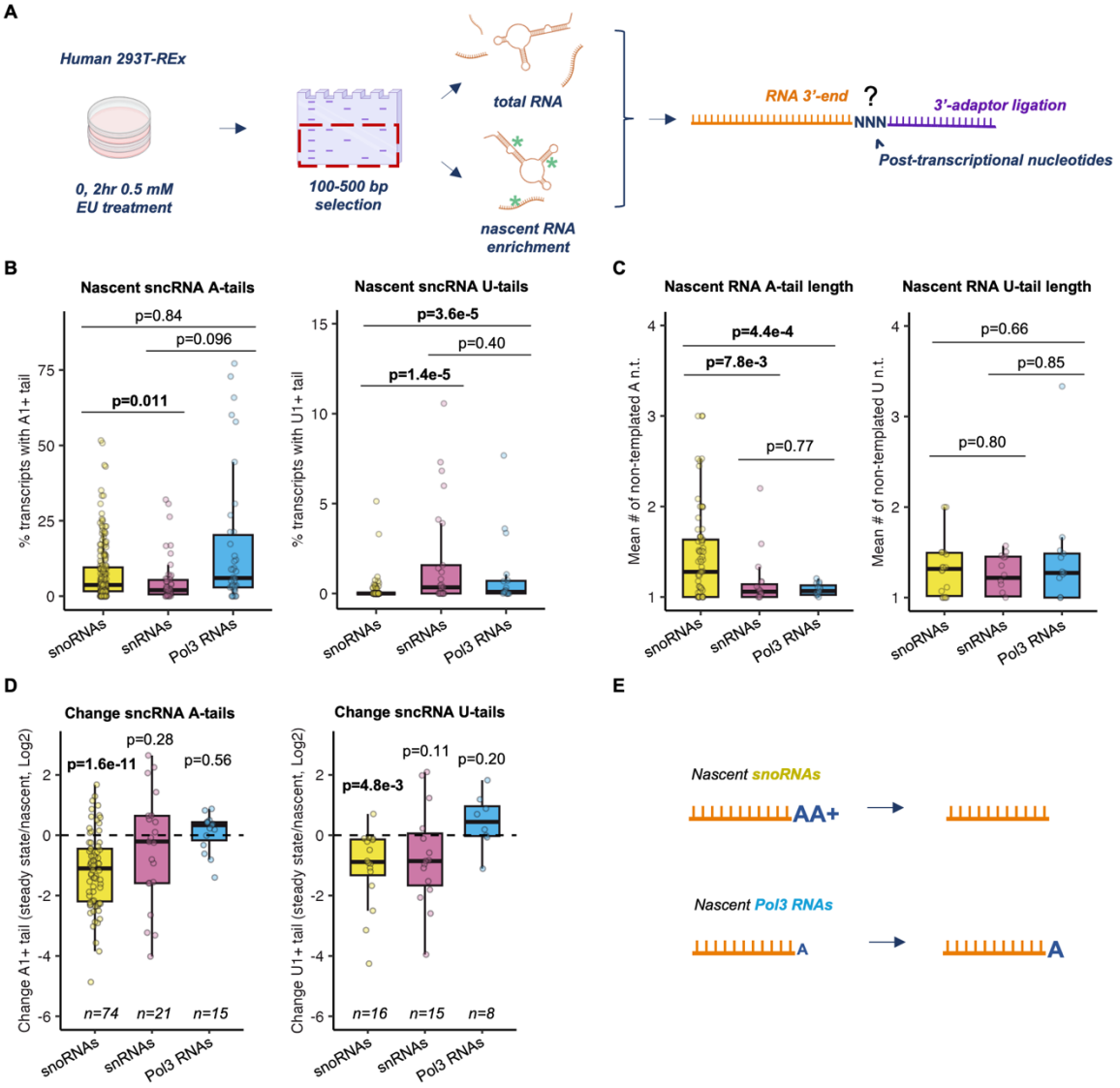

Figure 1. Post-transcriptional A- and U-tails are transient on a subset of sncRNAs but stable on others. (A) Schematic of the nascent and steady state sncRNA global 3′ end sequencing workflow. Human embryonic kidney (HEK) 293 T-REx cells were metabolically labeled with 5-ethynyluridine (EU) followed by RNA size-selection and nascent RNA capture. RNA 3′ ends were determined by global RNA 3' end sequencing of nascent and steady-state sncRNA samples in biological triplicate. Depictions of cell culture, gel extraction, and individual RNAs were created in BioRender (MO27QXAFOF, https://biorender.com/j15w879). **(B)** Percentage of nascent sncRNAs with A- (left) and U-tails (right). RNAs are grouped by their transcriptional origin and dots represent individual sncRNAs. P-values were determined by two-sample Kolmogorov-Smirnov (KS) tests, with $p<0.05$ shown in bold (snoRNAs n=98,

snRNAs n=25, Pol3 RNAs n=19). **(C)** Mean lengths of nascent sncRNA A- (left, snoRNAs n=74, snRNAs n=19, Pol3 RNAs n=15) and U-tails (right, snoRNAs n=18, snRNAs n=14, Pol3 RNAs n=13). P-values were determined by two-sample KS tests, with p<0.05 shown in bold. **(D)** Log2-fold ratios of percentages of A- (left) and U-tailed (right) sncRNAs in steady-state over nascent conditions. Transcripts with 0.1% or greater tailing in both nascent and steady state conditions were plotted. P-values were determined by a one-sample two-tailed t-test against mu=0, with p<0.05 shown in bold. **(E)** Schematic summarizing the 3'-end tail status of nascently-made snoRNAs and Pol-III RNAs. snoRNAs are modified with short oligo(A) tails which are absent in the steady state, while Pol-III RNAs retain their predominant mono(A) tails in the steady state. Depiction of RNA was created in BioRender (MO27QXAFOF, https://biorender.com/j15w879).

Figure 2 – Transient A-tailing is associated with destabilization for a population of snoRNAs

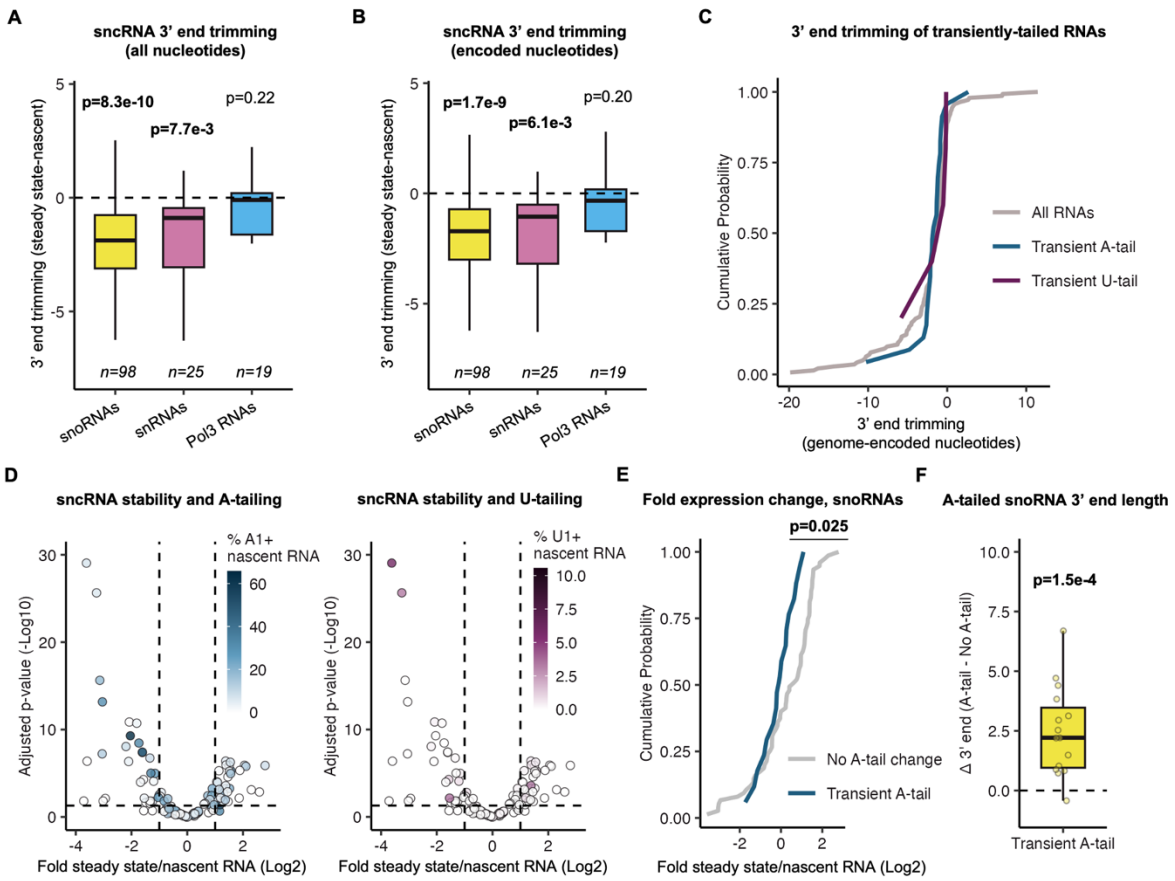

Figure 2. Transient A-tailing is associated with destabilization of snoRNAs. (A) and **(B)** Box plots showing ranges of sncRNA 3' trimming as measured by the difference in the mean 3′-end positions of transcripts in steady-state versus nascent RNA populations. Transcripts were binned by their transcriptional origin. Values in panel *B* excludes nucleotides from post-transcriptional tails. P-values were determined by a one-sample two-tailed t-test against mu=0, with $p<0.05$ shown in bold. **(C)** Cumulative plot showing sncRNA 3' trimming as measured by the difference in the mean 3′-end positions of transcripts in steady-state versus nascent RNA populations. SncRNAs that saw transient 3′ A-or U-tailing, as measured by a significantly ($p<0.05$; two-sample two-tailed t-test) higher fraction of A- or U-tailed molecules in nascent over steady state populations, are compared to all RNAs (All RNAs n=142, transient A-tails n=23, transient U-tails n=5). **(D)** Volcano plot comparing sncRNA stability with the percentages of A- (left) or U-tailed (right) molecules. The log2 fold ratio of sncRNA levels in steady-state over nascent conditions was quantified with DESeq2 and plotted against -log10-converted adjusted p-values. Individual sncRNAs are colored according to their percentage of modification with A- or U-tails of any length. The horizontal dashed line represents p=0.05. **(E)** Cumulative plot showing snoRNA stability as measured by the log2 ratio of steady-state over nascent levels. snoRNAs with significantly higher A-tailing in the nascent population relative to steady state are compared to all other snoRNAs. P-value was determined by a two-sample KS test (no A-tail change n=75, transient A-tail n=17). **(F)** Box plot showing the mean position of snoRNA A-tails relative to the 3' end position of their unadenylated counterparts for transiently A-tailed snoRNAs. P-value was determined by a one-sample two-tailed t-test against mu=0 (n=15).

Figure 3 – A subset of Pol-III RNAs and snRNAs stably accumulate with mono-A tails

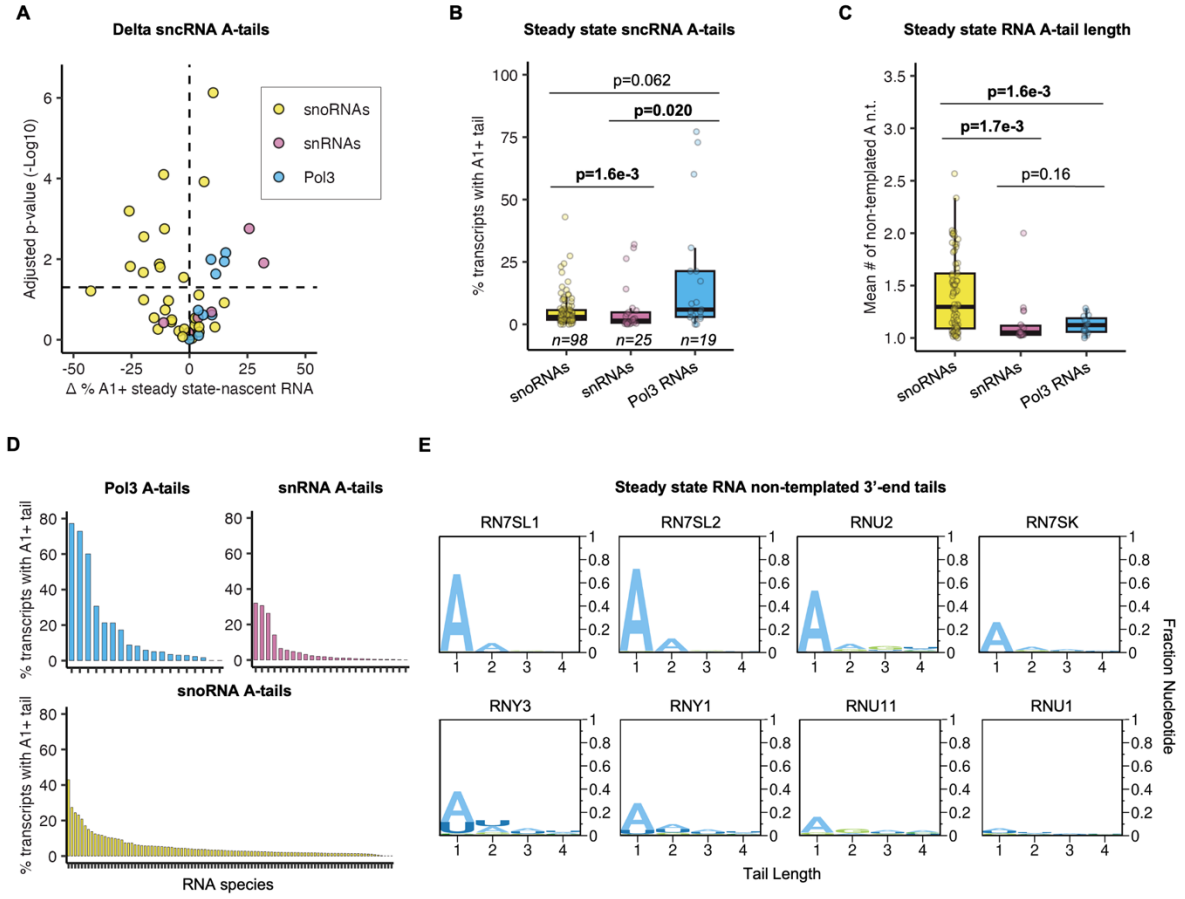

Figure 3. A subset of Pol-III RNAs and snRNAs stably accumulate with mono-A tails. (A) Volcano plot showing differences in percentages of A-tailed sncRNAs in the steady-state versus nascent conditions versus the -Log10 p-value of the difference. Only sncRNAs with ≥5% of the population with A tails in the steady state are plotted. Horizontal line indicates p=0.05 by a two-sample two-tailed t-test. Transcripts are colored by their transcriptional origin. **(B)** Box plots showing ranges in percentages of sncRNAs with A-tails at steady state. Transcripts were binned by their transcriptional origin. P-values determined by two-sample KS tests, with p<0.05 shown in bold. **(C)** The mean length of steady state A-tails of transcripts. Transcripts are binned by their transcriptional origin. P-values were determined by two-sample KS test, with p<0.05 shown in bold (snoRNAs n=74, snRNAs n=19, Pol3 RNAs n=15). **(D)** Rank order plot of sncRNAs by the percentage of the population with A-tails at steady state. Transcripts were plotted separately by their transcriptional origin. **(E)** Logo plots showing post-transcriptional tails at steady state for directly sequenced Pol-III RNAs and snRNAs. Post-transcriptional nucleotides are plotted as fractions of the total population.

Figure 4 – TENT2 contributes to Pol3 and snRNA 3' end A-tailing

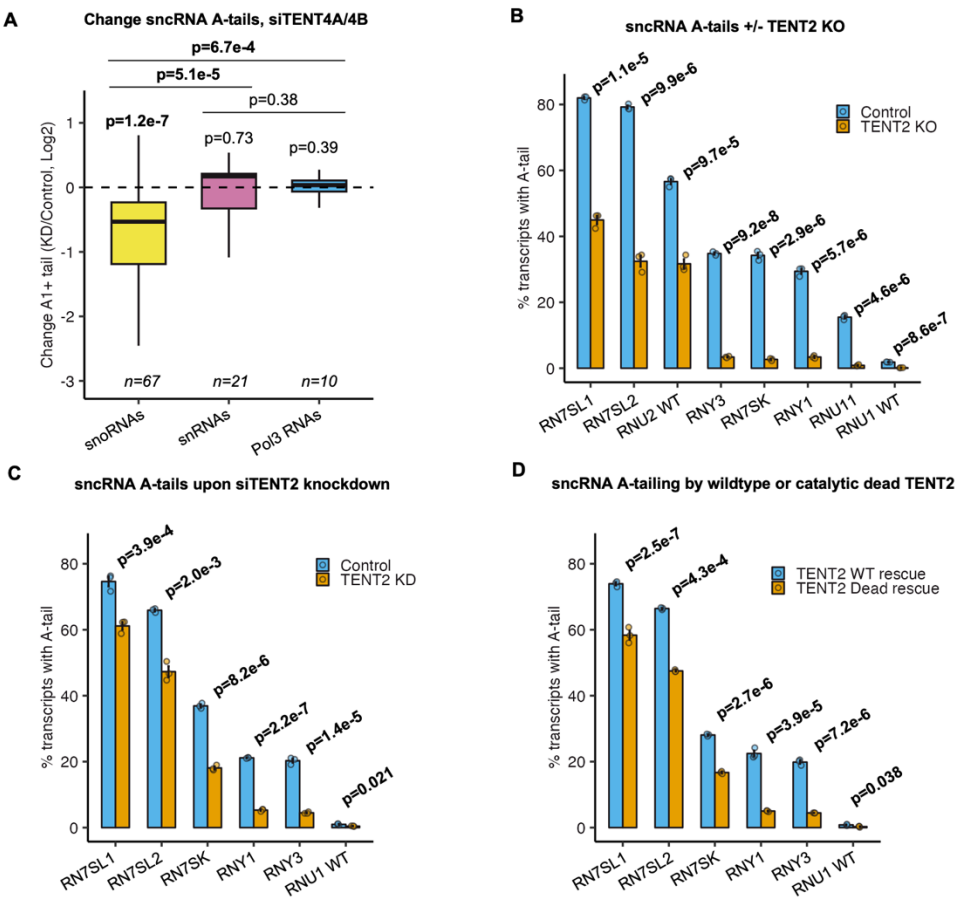

Figure 4. TENT2 contributes to Pol3 and snRNA 3' end A-tailing. (A) Box plots showing Log2 ratios in percentages of A-tailed sncRNAs in TENT4A/4B knockdown conditions over to control conditions. The dataset is from (Lim 2018). Transcripts are grouped by their transcriptional origin. P-values for individual groups were determined by one-sample two-tailed t-tests against mu=0. P-values between groups were determined by two-sample KS tests. p<0.05 is shown in bold. **(B)** Percentage of adenylated sncRNAs in TENT2 KO or control conditions in HEK 293T-Rex cells as measured for select Pol-III RNAs and snRNAs by gene-specific 3' end sequencing. Data is represented as mean +/- standard error of the mean (SEM) and p-values were determined by two-sample two-tailed t-tests, with p<0.05 shown in bold (n=3 for each transcript). **(C)** and **(D)** Percentage of adenylated sncRNAs in TENT2 siRNA depletion or control conditions in HEK 293T-Rex cells (panel *C*) or in TENT2-depleted HEK 293T-Rex cells complemented with TENT2 wild-type or TENT2 catalytic dead proteins (panel *D*). Data is represented as mean +/- SEM and p-values were determined by two-sample two-tailed t-tests, with p<0.05 shown in bold (n=3 for each transcript).

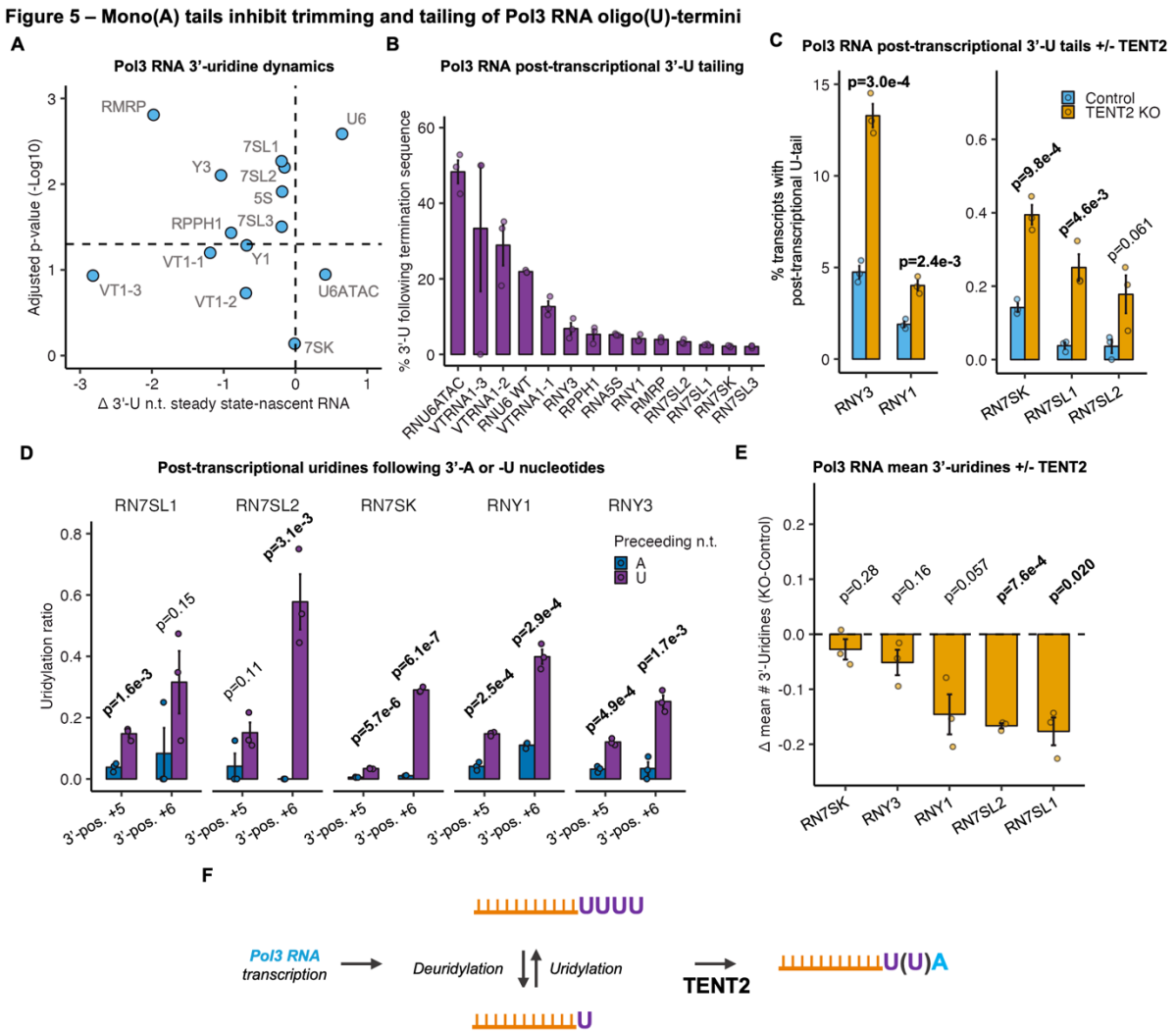

Figure 5. Mono(A) tails inhibit trimming and tailing of Pol3 RNA oligo(U)-termini. (A) Differences in lengths of 3′ uridine termini of steady state versus nascent Pol-III RNAs plotted against the -Log10 p-value for three independent experiments. P-values were determined by two-sample two-tailed t-tests. The horizontal line represents p=0.05 (n=3 for each transcript). **(B)** Percentage of Pol-III RNAs at steady state with post-transcriptional 3′-uridine(s) following the final uridine of their termination sequence. Data is represented as mean +/- SEM (n=3 for each transcript). **(C)** Percentage of Pol-III transcripts with post-transcriptional 3′-U tails in control or TENT2 KO conditions. Data is represented as mean +/- SEM and p-values were determined by two-sample two-tailed t-test, with p<0.05 shown in bold (n=3 for each transcript). **(D)** Ratio of post-transcriptional U nucleotides preceded by either A or U nucleotides plotted for 3′-end positions +5 and +6 relative to the first nucleotide of the termination sequence (defined as +1) so as to ensure a post-transcriptional origin of the uridine. Data is represented as mean +/- SEM and p-values were determined by two-sample two-tailed t-tests, with p<0.05 shown in bold (n=3 for each transcript). **(E)**

Difference in mean number of 3′-uridines of Pol-III RNAs between TENT2 KO and control cells. Data is represented as mean +/- SEM and p-values were determined by one-sample two-tailed t-tests against mu=0 with p<0.05 shown in bold (n=3 for each transcript). **(F)** Schematic representing uridine extension and trimming of nascent Pol-III RNAs which is terminated by monoadenylation by TENT2. Depiction of RNA was created in BioRender (MO27QXAFOF, https://biorender.com/j15w879).

Figure 6 – 7SL RNA association with La protein is impaired by TENT2

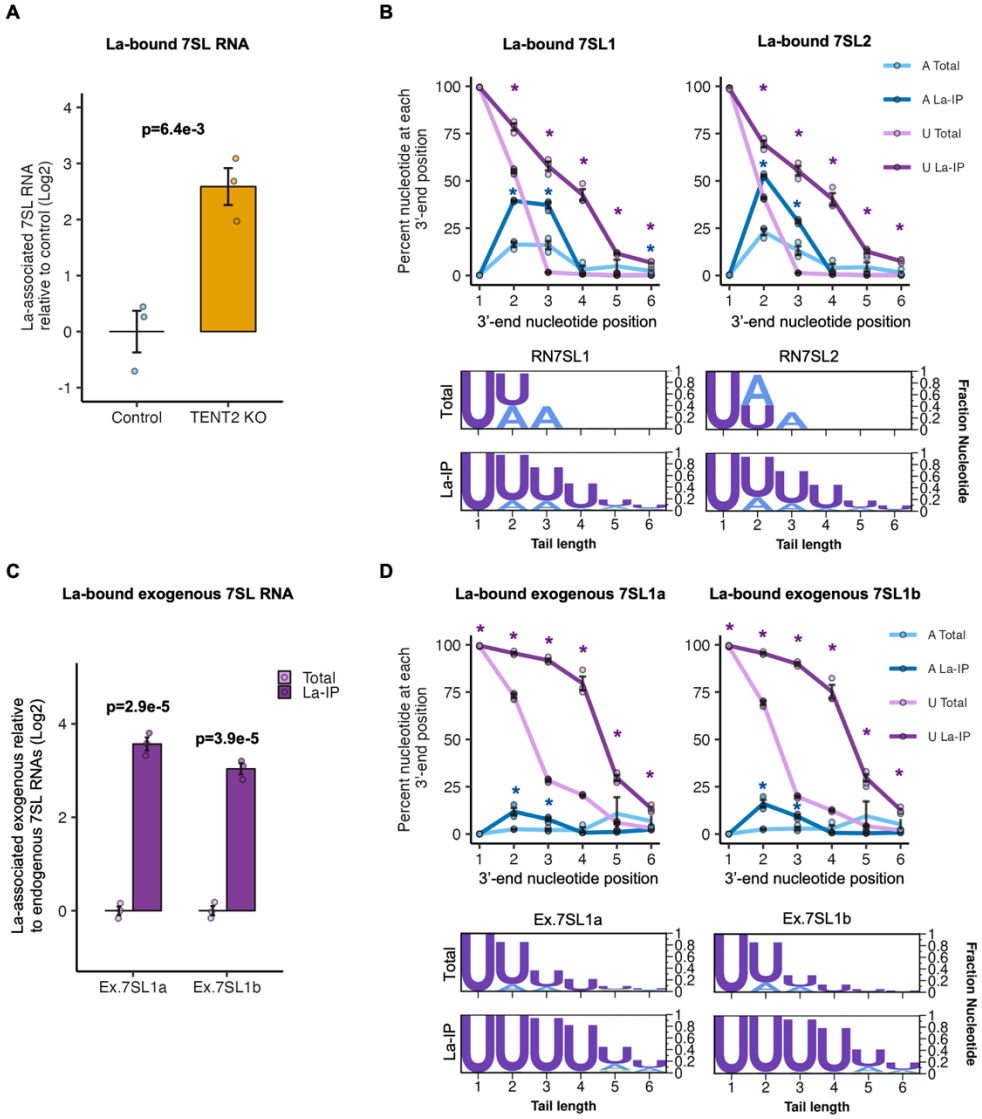

Figure 6. 7SL RNA association with La protein is inhibited by TENT2. (A) Levels of 7SL RNAs associated with La in control versus TENT2 KO conditions monitored by IP followed by

RT-qPCR for 7SL RNAs relative to U1 snRNAs and normalized against the IgG IP controls. Data is represented as mean +/- SEM and p-value was determined by a two-sample two-tailed t-test, with $p<0.05$ indicated in bold (n=3 for each condition). **(B)** 3' end nucleotide compositions of steady-state versus La-associated endogenous 7SL RNAs shown as line plots (top) and logo plots (bottom). Nucleotide positions are shown relative to the first nucleotide of the 7SL termination sequence, defined as position +1. Data is represented as mean +/- SEM and p-values between IP and input groups were determined by two-sample two-tailed t-tests, with $p<0.05$ indicated by asterisks (n=3 for each condition). Purple lines and asterisks represent U-tails, and blue lines/asterisks represent A-tails. **(C)** Levels of exogenous 7SL1a and 7SL1b RNAs associated with La relative to endogenous 7SL RNAs monitored by IP followed by sequencing. The relative abundance of exogenous 7SL1 RNAs bound to La was compared to the mean of endogenous 7SL1 and 7SL2 RNAs, then normalized to the relative abundance of exogenous U1 to endogenous U1. Data is represented as mean +/- SEM and p-values were determined by one-sample two-tailed t-tests against mu=0 with $p<0.05$ indicated in bold (n=3 for each condition). **(D)** Same analysis as panel *B*, but monitoring exogenous 7SL1 RNAs.

Figure 7 – Excessively uridylated 7SL RNAs are impaired in the final step of SRP assembly

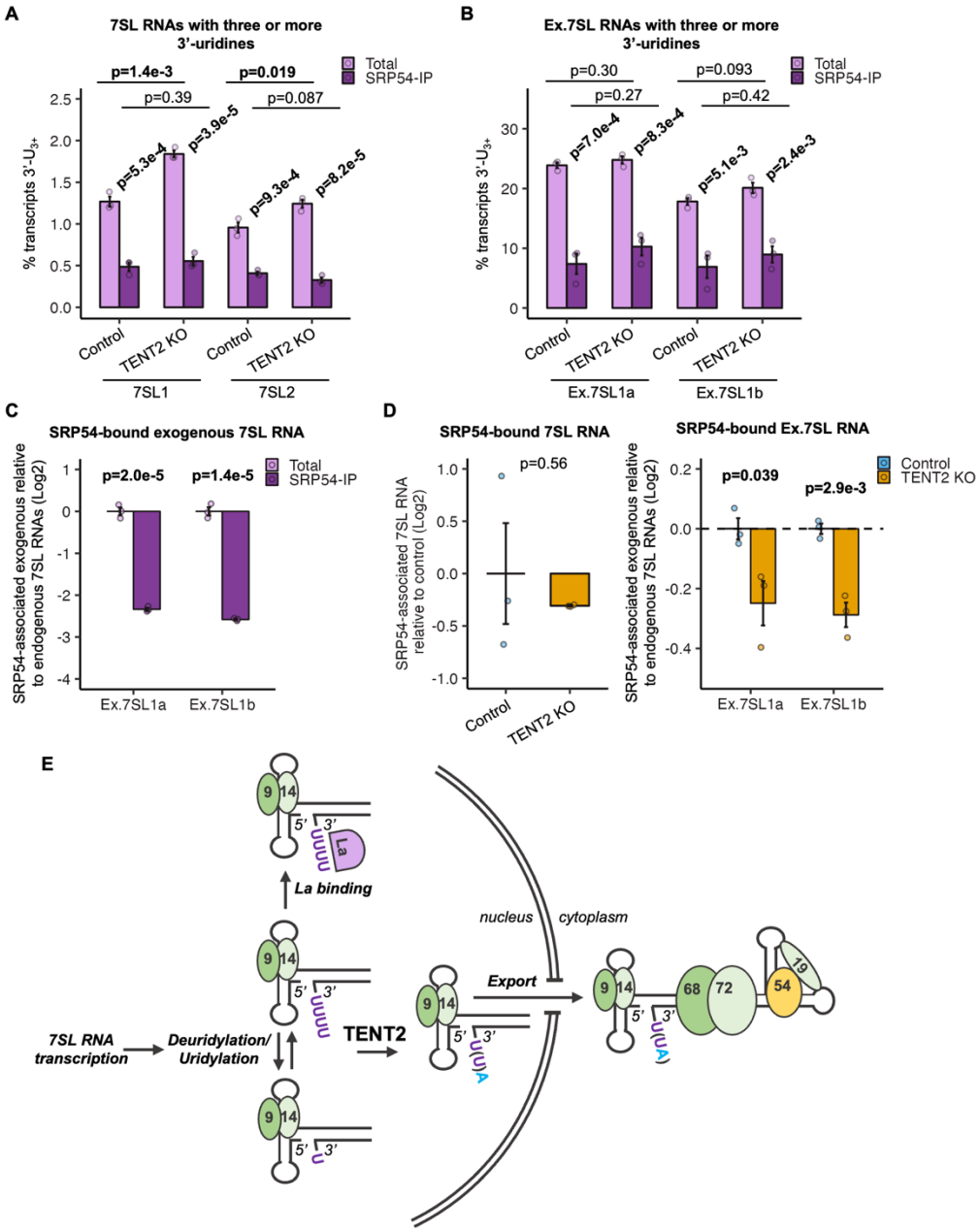

Figure 7. Excessively uridylated 7SL RNAs are impaired in the final step of SRP assembly. **(A)** Percentage of endogenous 7SL RNAs with 3 or more 3′-uridines in input versus SRP54-IP conditions and control versus TENT2 KO conditions. Data is represented as mean +/- SEM and p-values were determined by two-sample two-tailed t-tests, with p<0.05 indicated in bold (n=3 per condition). **(B)** Same as panel *A* but monitoring exogenous 7SL RNAs. **(C)** Log2 ratio of SRP54-associated exogenous 7SL1 RNAs over endogenous 7SL RNAs, monitored by sequencing. Data is represented as mean +/- SEM and p-values were determined by one-sample two-tailed t-tests against mu=0 with p<0.05 indicated in bold (n=3 for each condition). **(D)** Impact of TENT2 KO on 7SL RNA association with SRP54. Left: levels of SRP54-associated 7SL RNAs monitored by IP followed by RT-qPCR for 7SL RNAs relative to U1 snRNAs and

normalized against the average level of association in the absence of TENT2 KO (control). Data is represented as the log2 mean +/- SEM and p-value was determined by a two-sample two-tailed t-test, with $p<0.05$ indicated in bold (n=3 per condition). Right: log2 ratio of exogenous 7SL1 RNAs over endogenous 7SL RNAs in SRP54 IP samples in control and TENT2 KO conditions monitored by sequencing and normalized against the average association ratio in the absence of TENT2 KO (control). Data is represented as the log2 mean +/- SEM and p-values were determined by two-sample two-tailed t-tests, with $p<0.05$ indicated in bold (n=3 for each condition). **(E)** Schematic representing stages of 7SL biogenesis. 7SL RNAs with 3 or more uridines may be bound by La. TENT2 adenylates 7SL 3′ ends which promotes release from La, allowing nuclear export and assembly of SRP in the cytoplasm with SRP54.